J. Fluid Mech. (1980), *vol.* 99, *part* 1, *pp.* 53–64
Printed in Great Britain

A visual investigation of turbulence in stagnation flow about a circular cylinder

By WILLY Z. SADEH AND HERBERT J. BRAUER
Colorado State University, Fort Collins, Colorado 80523

(Received 30 June 1978 and in revised form 29 October 1979)

A diagnostic visualization study of turbulence in stagnation flow around a circular cylinder was carried out to gain physical insight into the coherent structure of turbulence in flow around a bluff body advanced by the vorticity-amplification theory. The visualization was conducted at a cylinder-diameter Reynolds number of 8×10^3 utilizing titanium dioxide white smoke for an approaching flow containing turbulence at scales larger than the neutral wavelength of the stagnation flow. Analyses of the flow events focused on tracing out the temporal and spatial evolution of a cross-vortex tube outlined by the entrained smoke filaments from its emergence near the stagnation zone through its penetration into the cylinder boundary layer.

The selective stretching of cross-vortex tubes, their streamwise tilting, the emergence of an organized turbulent flow pattern near the stagnation zone, the interaction of the amplified vorticity with the body laminar boundary layer and the growth of a turbulent boundary layer were revealed by the visualization. In particular, the visualization indicated that the cross-vortex tubes conveyed by the diverging stagnation flow constitute a coherent substructure within the overall turbulent flow that is triggered to its fullest manifestation by the stretching mechanism.

1. Introduction

The importance of turbulence amplification in the flow approaching the stagnation zone of a bluff body is currently recognized. Results of many investigations, both experimental and theoretical, clearly attest to the strong sensitivity of both stagnation-point skin friction and heat transfer to the presence and, particularly, the nature of the oncoming turbulence. Occurrence of relatively large velocity fluctuations upstream of the stagnation zone of a circular cylinder and of an airplane strut was first reported by Piercy & Richardson (1928, 1930). A discussion of the earlier background of this flow situation can be found in a report by Kestin & Maeder (1957). Additional history on this subject is available in papers by Sutera, Maeder & Kestin (1963), Sutera (1965), Sadeh, Sutera & Maeder (1970*a*, *b*), and in numerous other papers (e.g. see: Kestin 1966; Kestin, Brun & Diep 1966; Kestin & Wood, 1970; Bearman 1972; Hunt 1973; Traci & Wilcox 1975). A thorough survey of this flow is not given herein since the background literature is readily accessible. The vorticity-amplification theory is, however, briefly reviewed for the sake of laying down the guidelines regarding this visualization study.

0022–1120/80/4468–1170 $02.00

2. Vorticity-amplification theory

The vorticity-amplification theory advanced by Sutera *et al.* (1963) and further extended by Sadeh *et al.* (1970*a*) offers a satisfactory explanation for the evolution of turbulence in flow around a bluff body and its three-dimensional effects on the stagnation-point boundary layer. This theory suggests that specific turbulent fluctuations present in the on coming stream, no matter how small initially, are susceptible to undergoing significant amplification as they are conveyed by the diverging mean flow toward the body stagnation zone. Selective stretching of cross-vortex filaments is proposed as the mechanism responsible for the amplification of cross vorticity and, hence, of streamwise turbulence. Relatively high levels of turbulent energy concentration emerge near the stagnation zone at particular scales λ greater than a certain neutral scale λ_0 as a result of the vorticity amplification. At these scales the vorticity increases in amplitude more rapidly than it dissipates by viscous action. The intensified turbulence concentrated at these scales is the agent causing the observed increases in shear stress and heat transfer at the wall. At scales smaller than the neutral one the viscous dissipation is the main effect while a balance between the vorticity amplification and the viscous dissipation prevails at the neutral scale λ_0.

The stretching and tilting of vortex filaments and their viscous diffusion are accounted for in the vorticity transport equation. For the flow of a viscous, incompressible fluid of constant properties the vorticity transport equation in Cartesian tensor notation is

$$\frac{D\omega_i}{Dt} = \omega_j \frac{\partial U_i}{\partial x_j} + \nu \frac{\partial^2 \omega_i}{\partial x_j \partial x_j}, \tag{1}$$

in which ω_i and U_i designate the total vorticity and velocity (mean plus fluctuating values) and ν stands for the kinematic viscosity of the fluid. Axial stretching (or squeezing) of vortex filaments along their axes is outlined by the three terms $\omega_j \partial U_i/\partial x_j$ when $i = j$ whereas tilting is represented by the six terms $\omega_j \partial U_i/\partial x_j$ when $i \neq j$.

Cross flow about an infinitely long circular cylinder of radius R neglecting viscous dissipation is examined for outlining the stretching and tilting mechanisms. This flow situation together with the system of co-ordinates used is portrayed in figure 1. It is assumed that the approaching total velocity U_2 contains mainly cross vorticity ω_1 susceptible to undergoing stretching in the diverging stagnation-point flow around the cylinder. A single ideal cross-vortex tube whose vorticity is ω_1 and of a scale λ larger than the neutral scale λ_0 is considered in the x_1, x_2 plane (the stream plane) at some upstream station x_2^0 as depicted in figure 1. This cross-vortex tube undergoes simultaneous pure axial stretching and streamwise biased tilting as it is swept by the mean flow towards the stagnation zone. The pure axial stretching is controlled by the positive rate of tensile strain $\partial U_1/\partial x_1$. Concurrently, the streamwise biased tilting is governed by the suitable rate of cross strain $\partial U_2/\partial x_1$ whose magnitude increases in the x_1 direction ($\partial U_2/\partial x_1 > 0$). Both these two favourable rates of strain, which are shown in figure 1, are effected by the diverging stagnation flow. It is further important to point out that a cross-vortex tube experiences additional axial stretching and acquires a vorticity component ω_2 in the x_2 direction owing to its streamwise biased tilting as it approaches a body. The axial stretching and the streamwise biased tilting of a cross-vortex fila-

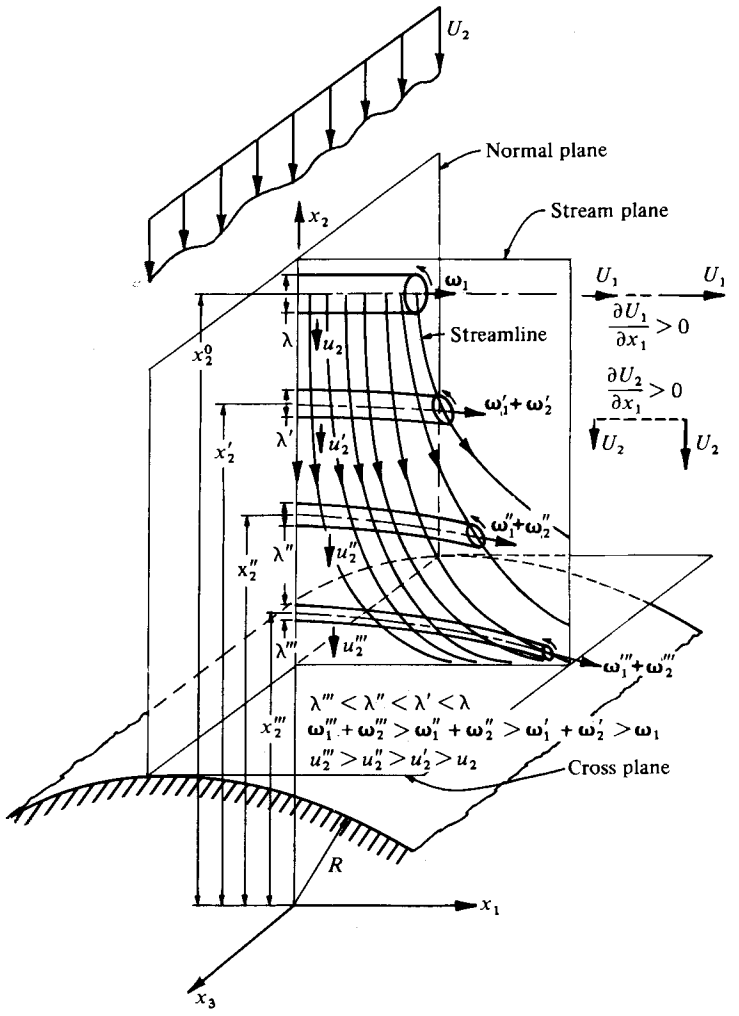

FIGURE 1. Illustration of the stretching and tilting of a cross-vortex tube.

ment, initially at an upstream station x_2^0, are illustrated in figure 1 at three streamwise stations x_2', x_2'' and x_2''' as it nears a body.

The volume and the angular momentum of each cross-vortex filament are conserved throughout the stretching as a result of disregarding the viscous dissipation. Stretching of a cross-vortex tube is consequently accompanied by a decrease in its scale (or diameter) λ and by an increase in its vorticity (or angular velocity) ω. Then the streamwise turbulent velocity u_2 in the plane normal to the axis of the cross-vortex tube amplifies and turbulent kinetic energy concentrates within the stretched cross-vortex filaments. The decrease in the scale and the accompanying increase in the vorticity of a cross-vortex tube approaching a body along with the amplification of the streamwise turbulent velocity is portrayed in figure 1 at three streamwise stations x_2', x_2'' and x_2''', viz. $\lambda''' < \lambda'' < \lambda' < \lambda$, $\boldsymbol{\omega}_1''' + \boldsymbol{\omega}_2''' > \boldsymbol{\omega}_1'' + \boldsymbol{\omega}_2'' > \boldsymbol{\omega}_1' + \boldsymbol{\omega}_2' > \boldsymbol{\omega}_1$ and $u_2''' > u_2'' > u_2' > u_2$, where the initial values at station x_2^0 are unprimed. One can view the cross-vortex

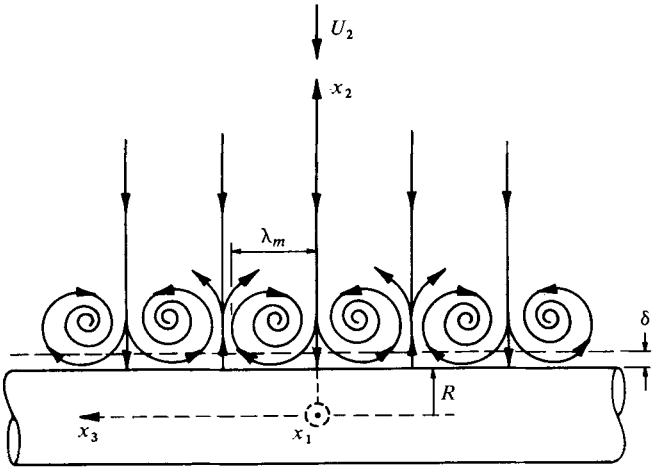

FIGURE 2. Theoretical coherent vortex flow pattern near the stagnation zone.

tubes being conveyed by the diverging stagnation flow as an organized substructure subsisting within the overall random turbulent field. The stretching represents the triggering agent needed to unfold this latent coherent substructure to its fullest manifestation. It is important to point out that the stretching and tilting act simultaneously as a cross-vortex tube approaches a body. The turbulence amplification process starts at an upwind distance much larger than the body boundary-layer thickness and it is therefore not associated with any instabilities within the body boundary layer.

The stretching and tilting lead to the development of an organized cellular flow pattern near the stagnation zone of a body. This coherent substructure consists ideally of a regular array of standing cross-vortex tubes of equal scale distributed spanwise with their axes parallel to the streamlines along the body and with their cores outside the body boundary layer as illustrated in figure 2. Within the cells of this orderly array the rotation alternates in its direction and turbulent energy accumulates. Most of the turbulence amplification occurs at a most amplified scale λ_m (Sadeh *et al.* 1970*b*) which is generally greater than but commensurate with the body boundary-layer thickness δ. Discrete vortices (or eddies) are continuously drawn out from this array of standing vortexes and, subsequently, swept downstream by the main flow round the body. They are able to penetrate into the prevailing boundary layer and to affect its properties. A supply of adequately amplified turbulence can lead to arresting the growth or even to the forestalling of laminar separation by fostering the development of a turbulent boundary layer. One can thus affect the nature of the body boundary layer in a controlled way provided that the turbulence amplification is properly managed by the stretching and tilting mechanisms.

An extensive, albeit not exhaustive, visualization of the flow near the stagnation zone of a circular cylinder was conducted to obtain a physical insight into the overall flow structure. Digitization of the flow images was sought for estimating the time and space evolutions of the flow patterns and their significant scales.

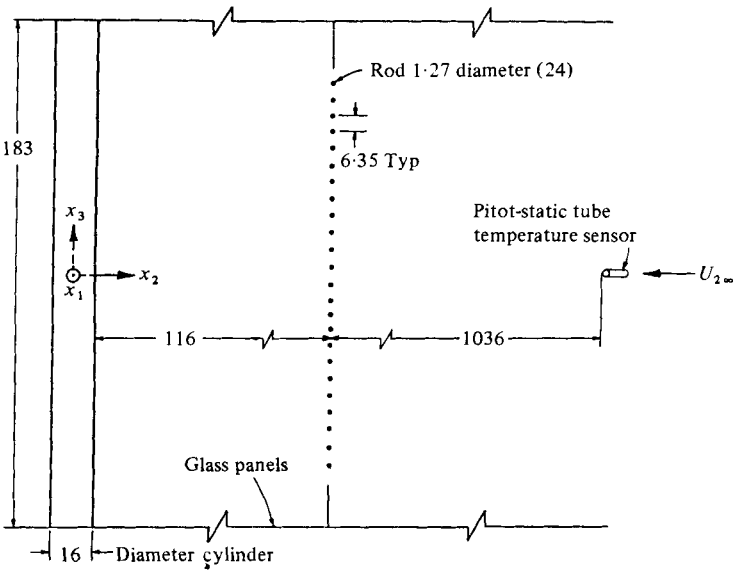

FIGURE 3. Sketch of experimental arrangement in the wind tunnel. All dimensions in cm.

3. Experimental set-up

The flow visualization was conducted in a $1{\cdot}83 \times 1{\cdot}83 \times 27$ m ($6 \times 6 \times 88$ ft) low-speed closed-circuit single-return wind tunnel at the Fluid Dynamics and Diffusion Laboratory, Colorado State University. Throughout the flow visualization the free-stream velocity $U_{2\infty}$ was maintained at 0·76 m s^{-1} within a resolution of about 35 %. A circular cylinder 16 cm in diameter D and 1·83 m long made of light aluminium alloy painted with dead-black lacquer was used. It was mounted across the width of the wind tunnel 23 m downstream of the test-section entrance with its axis 0·61 m above the floor. Its blockage coefficient was about 0·087. A schematic diagram of the experimental arrangement (top view in the x_2, x_3 plane) including all important dimensions and the system of co-ordinates used is displayed in figure 3.

The visualization was carried out at a cylinder-diameter Reynolds number

$$Re_D = 8 \times 10^3$$

based on the free-stream velocity (air at 20 °C, kinematic viscosity

$$\nu = 1{\cdot}5 \times 10^{-5}\,\mathrm{m^2\,s^{-1}}).$$

At this Reynolds number, a neutral wavelength (Sadeh *et al.* 1970*a*)

$$\lambda_0 = \pi D/Re_D^{\frac{1}{2}}, \tag{2}$$

and a laminar boundary-layer thickness

$$\delta = 1{\cdot}2D/Re_D^{\frac{1}{2}}, \tag{3}$$

of 5·6 and 2·15 mm, respectively, were expected.

Controlled production of free-stream turbulence (or vorticity) was achieved utilizing a turbulence-generating grid consisting of 24 regularly spaced vertical cylindrical bars that spanned the entire height of the wind-tunnel cross-section. The vertical direction of the rods was specifically selected for generating vorticity oriented mainly in the x_1 direction. Aluminium rods, each 1·27 cm in diameter d, spaced at centre-to-centre intervals of 6·35 cm were employed. The grid Reynolds number, based on the grid mesh (5 cm) and the free-stream velocity, was about 2600. This grid was installed 116 cm upwind of the cylinder as shown in figure 3 (at an upstream distance of $7{\cdot}32D$ or $91{\cdot}5d$).

The Reynolds number of each rod of the grid, based on the free-stream velocity and/or the velocity immediately downstream of the grid (20 % blockage) and the rod diameter d, was about 650 or 780. At these Reynolds numbers, the Strouhal number S (i.e. $S = nd/U_2$, where n is the frequency) is 0·21 (Roshko 1954). Most of the turbulent energy was consequently concentrated at a Strouhal frequency of about 12·6 Hz. The Strouhal scale $\lambda_S = U_2/n$, approximated under the frozen-pattern assumption (Taylor 1938), was 60·45 mm. Free-stream turbulence was thus mainly produced at a scale almost 11 times greater than the neutral scale of the stagnation flow.

4. Experimental procedure

The free-stream velocity was monitored by means of a Pitot-static tube located 10·36 m (34 ft) upwind of the turbulence-generating grid in the plane $x_3 = 0$ as indicated in figure 3. No viscous correction was necessary at the low free-stream velocity used since the tube Reynolds number, based on its outside radius (1·6 mm), was about 80 (Hurd, Chesky & Shapiro 1953). Furthermore, the reading of the Pitot-static tube was not affected by the superimposed turbulence as it was positioned upstream of the turbulence-generating grid, where the wind-tunnel background turbulence intensity is of the order of 0·74 % (Dean 1955; Ower & Pankhurst 1966). The dynamic pressure was measured with a resolution of 0·0005 mmHg. Simultaneously, the stream temperature was continuously monitored in the same plane as the Pitot-static tube with a resolution of 0·1 °C. At the midpoint between the grid and the cylinder, the turbulence intensity, based on local mean velocity, was about 7·7 %. All the turbulence intensities were measured by means of a hot-wire anemometer.

The flow visualization was carried out utilizing titanium dioxide (TiO_2) white smoke that was produced by mixing moist compressed air with titanium tetrachloride. Smoke was injected through a single and/or two brass tubes connected through Tygon tubes to the smoke generators. The Reynolds number of each tube, based on its outside radius (1·6 mm) at the prevailing free-stream velocity, was about 80. Consequently, the tube wake effect upon the smoke flow was completely negligible. All the tubes were positioned 5 cm upstream of the cylinder in the plane $x_1 = 0$ (i.e. in the normal plane, see figure 1) at angles of either 0 or 30° with respect to the x_2 axis. The positioning of the smoke injection tubes was determined, after a series of checks in an approaching laminar flow (no grid), in order to minimize any tube interference effect on the flow. Extreme care was taken to match the smoke exit velocity to the prevalent stream velocity for ensuring its neutral entrainment.

Colour 16 mm movies were shot at a speed of 24 frames per second and, therefore, the time interval of each individual frame was $41\frac{2}{3}$ ms. Lighting was supplied by means of

four adjustable floodlights and spotlights of fixed and/or variable focus. Light sheets were produced, whenever necessary, using their built-in barn doors. The composition of the lamps and their light intensity were adjusted in each photographic situation for enhancing the illumination of the smoke and for minimizing the glare induced by the smooth surface of the cylinder.

5. Examination of flow events

The main objectives of the flow visualization study were: (1) demonstration of the stretching of cross-vortex tubes; (2) illustration of the tilting of cross-vortex tubes; (3) delineation of the coherent vortex substructure near the stagnation zone of the cylinder; (4) identification of the interaction between the amplified turbulence and the cylinder laminar boundary layer; and (5) outlining the development of a turbulent boundary layer. In order to achieve these aims, the smoke patterns were photographed from three viewpoints, viz. side, top and rear views (in planes x_1x_2, x_2x_3 and x_1x_3; see figure 1). The visualization study reported herein was confined to a single Reynolds number (8×10^3) owing to time constraints. Preliminary surveys at other Reynolds numbers revealed a similar turbulent flow pattern as the one discussed herein.

An overall examination of more than 610 m (2000 ft) of movies was carried out. Static presentation of stills from movie strips, as discussed herein, cannot match the dynamic impact conveyed by the motion pictures. A summary movie 10 minutes 53 seconds long entitled 'Vorticity Amplification in Stagnation Flow About a Circular Cylinder' that incorporates the most instructive views was edited and is available for loan.†

The task at hand was both the qualitative and quantitative interpretation of the motion pictures for the sake of ascertaining the development in time and space of the flow pattern. Extreme care was exercised in analysing selected movie strips owing to the inherent restrictions that stem from their instantaneous interpretation and two-dimensionality. Each single frame, whose significant size was about $10 \times 7{\cdot}5$ mm (width × height), was magnified 61 times and inspected with the aid of a photo-optical data-analyser ciné projector that permitted a complete stopping of the action indefinitely at any desired frame for close examination and digitization.

The pattern of the smoke filaments entrained by a cross-vortex tube was tracked for each single frame on its magnified image. Interpretative sketches of sequences up to, at most, 20 frames (i.e. over a time interval up to $833\frac{1}{3}$ ms) were edited for each particular view angle. The pathlines are traced in these sketches by solid lines and the rotation direction is indicated by an arrow. In ditigizing the smoke pattern, a length scale was estimated in each case based on the known upstream distance of the smoke injection tube (5 cm; see §4). The scale, the time axis (t axis), the time interval of each frame, the frame counter N, the system of co-ordinates and the total approaching velocity are shown in all the sketches of the flow patterns. In addition, the theoretical laminar boundary-layer thickness (2·15 mm; see §3) is indicated in all the sketches by a dashed line and the letter L. The cylinder itself is marked off in the schematic diagrams by a solid line. In carrying out the analysis of the flow images, the effects of viscous dissipation were neglected since the primary objective was to demonstrate the stretching and tilting mechanisms and their consequences.

† At this time the movie can be obtained by contacting Professor Willy Z. Sadeh.

5.1. *Side views*

The time history or 'life cycle' of a cross-vortex tube from its 'embryo', throughout its 'maturing' and until its 'ageing' was distinctly perceived in the side-view motion pictures, i.e. views in the x_1, x_2 plane (the stream plane). A sequence of 18 representative frames extending over a time span of 750 ms together with their corresponding schematic diagrams are shown in figures 4 (*a*)–(*e*) (plates 1–5). Note that the mirror image of the smoke pattern is reflected on the cylinder surface. In these figures *S* designates side view and the scale of the sketches is 1:3. The thickening of the theoretical laminar boundary layer along the cylinder circumference from 2·15 mm at the stagnation zone up to about 6 mm at an angle of 70–80 degrees (measured from the stagnation point) is outlined in all the sketches (Schlichting 1968). In determining the life cycle of a cross-vortex tube, the vestiges of the smoke filaments entrained by a previous cross-vortex tube were disregarded in tracing out the flow patterns although they are clearly identified in the flow images.

The initial and the subsequent gradual entrainment of the approaching smoke filaments into an emerging cross-vortex tube near the stagnation zone is noticed in the first four frames, viz. in frames 1-*S* to 4-*S* up to $t = 166\frac{2}{3}$ ms (figure 4*a*). Subsequently, the maturing process of the cross-vortex tube and its axial stretching in the x_1 direction become prominent starting from $t = 208\frac{1}{3}$ ms (frame 5-*S*, figure 4*b*). A clearly outlined stretched cross-vortex tube is finally observed in frames 5-*S* to 9-*S* ($t = 208\frac{1}{3}$ to 375 ms, figures 4*b*, *c*).

The spatial scales of the cross-vortex tubes, i.e. their width in the stream plane approximated according to the specified scale, ranged roughly from 4 to 40 mm as indicated in the schematic diagrams of the pathlines (figures 4*a–e*). In the sketches the largest scale of the tube (or its envelope) is marked by a broken line (– · –). Vorticity at scales larger than the neutral scale (5·6 mm; see equation (2)) prevailed, therefore, near the stagnation zone. This is exactly the cross vorticity that undergoes amplification by stretching. Occurrence of selective stretching of cross-vortex tubes is thus substantiated by the observed flow pattern. The scales of the stretched cross-vortex tube are larger than the thickness of the laminar boundary layer and its core is clearly outside the boundary layer.

Tilting in the streamwise direction of the tracked cross-vortex tube is noticed during its maturing phase in the stills shown in figures 4 (*b*)–(*d*). The start-up of the vortex-tube tilting is indicated by the winding of the smoke filaments over the cylinder that is perceived starting from $t = 250$ ms (frame 6-*S*, figure 4*b*). As the stretched tube moves downstream, the tilting becomes more pronounced with increasing time. The tilting is further accompanied by a continuous expansion of the cross-vortex tube. For instance, the gross scale expands from about 18 mm at $t = 250$ ms (frame 6-*S*, figure 4*b*) to roughly 40 mm at $t = 666\frac{2}{3}$ ms (frame 16-*S*, figure 4*d*). The systematic biasing of the tilting in the streamwise direction is thus unveiled by the visualized flow pattern.

The penetration of the amplified vorticity (or amplified turbulence) into the laminar boundary layer at the stagnation zone is perceived beginning from about $t = 125$ to $166\frac{2}{3}$ ms (frames 3-*S* to 4-*S*, figure 4*a*). As the interaction with the boundary layer progresses, the distortion of the flow pattern within a continuously distending vortex tube becomes more conspicuous as observed starting from about $t = 333\frac{1}{3}$ to 375 ms (frames 8-*S* and 9-*S* figures, 4*b*, *c*). The agitated state of the smoke filaments unravelled

by the prevailing spiral pattern is the prominent feature of the distorted flow shown in sketches 13-S to 16-S ($t = 541\frac{2}{3}$ to $666\frac{2}{3}$ ms, figure 4d). This overall disordered pattern of the smoke filaments testifies to the development of a turbulent boundary layer.

As the interaction of the stretched cross-vortex tube with the boundary layer progresses, the vortex tube ages and gradually loses its identity. Simultaneously, another similar cross-vortex pattern shows up near the stagnation zone and enters upon a similar sequence of events. Both the ageing of the tracked tube and the onset of another cross-vortex tube near the stagnation zone are identified starting from $t = 541\frac{2}{3}$ ms (frame 13-S, figure 4b). The large scale of the newly emerging cross-vortex tube is about 15 mm (frames 17-S and 18-S, figure 4e) and, thus, it is roughly of the same size as that of the ageing one at about a corresponding stage in its growth (see frame 7-S, figure 4b). It is, hence, apparent that the life cycle of a vortex tube extends over a time interval of about 750 ms at the particular Reynolds number (8×10^3) for this flow situation. Analysis of other side-view sequences confirmed this time span within $\pm$ 5–10 %.

5.2. *Top views*

Top-view motion pictures were taken directly above the stagnation zone in the x_2, x_3 plane (the normal plane) in order to visualize the coherent vortex substructure near the stagnation zone. A sequence of 20 stills, $833\frac{1}{3}$ ms long from a selected movie strip, and their digitized sketches are displayed in figures 5(a)–(e) (plates 6–10). In these figures T stands for the top view and the scale of the schematics is 6:5. The analysis of the top-view sequence focused on ascertaining the significant scales of a standing cross-vortex tube and the changes with time of its shape.

A standing cross-vortex tube whose axis is in the x_1 direction and with its core outside the laminar boundary layer is exhibited by the vortex flow pattern over the entire time span of $833\frac{1}{3}$ ms. This time span was estimated based on tracking the successive changes in the pathlines starting with a reasonably defined regular vortex pattern close to the body until the recurrence of a roughly similar pattern at about the same spatial position. In comparing frames 1-T ($t = 41\frac{2}{3}$ ms, figure 5a) and 20-T ($t = 833\frac{1}{3}$ ms, figure 5e), which are $791\frac{2}{3}$ ms apart, one can observe that the pathlines of the entrained smoke are similar in their almost regular pattern and that the leading edge of both vortex tubes is roughly at the same distance of 5 mm upstream of the cylinder.

A rapid decrease in the scale of the cross-vortex tube across and down its 'barrel', i.e. along its axis in x_1 direction, is readily perceived in the top images. This diminution in the scale is accompanied by an augmentation in the angular velocity according to the conservation of angular momentum. A gradual increase in the smoke rotational velocity is, in fact, vividly perceivable elsewhere in the motion pictures. The continuous scale decrease and the accompanying increase in the rotational velocity along the shrinking pathlines that are observed at all times attest the preferred stretching experienced by the cross-vortex tubes.

Scales of selected pathlines, derived according to the prescribed scale, ranged from about 2 to 32 mm. They are generally greater than the neutral wavelength. The scales smaller than the neutral one outline cross-vortex tubes whose energy balance is dominated by viscous dissipation. Assessment of the most amplified scale directly from the flow images is not feasible since its determination is contingent upon measuring the turbulent energy distribution.

Penetration of the large-scale vorticity into the stagnation laminar boundary layer is discerned starting from $t = 125$ ms (frame 3-T, figure 5a) and it is seen to last until $t = 625$ ms (frame 15-T, figure 5d) in the life cycle. The tilting and wrapping of vortex tubes around the cylinder is represented in the top views by the smoke streamers carried over and underneath it. They are delineated in the schematic diagrams by a double broken line (– – · – –) and a simple broken line (– · –), respectively.

In comparing the shape of the cross-vortex tube at $t = 41\frac{2}{3}$ ms (frame 1-T, figure 5a) and $208\frac{1}{3}$ ms (frame 5-T, figure 5b), it is evident that its initial regular form experiences severe distortions. Looking closely at frames 5-T to 19-T (figures 5a–e), one can detect that these contortions are primarily sustained by the large scale of the cross-vortex tube while its smaller scales are much less affected. These distortions are attributed to the continuous interaction among the standing cross-vortex tubes distributed along the span of the stagnation zone within which the rotation repeatedly changes its direction as portrayed in figure 2. This vortex interaction is illustrated in sketch 10-T (figure 5c) in which two adjacent standing tubes are depicted by a dashed line in addition to the visualized cross-vortex tube. Based on the continuously changing pattern of the embayments of the tube interface (the large scale) it is apparent that the rotation within both the contiguous left-hand and right-hand tubes is in a counterclockwise direction. These two tubes are, in turn, distorted by the one located in between them within which the rotation is in a clockwise direction as perceived in the displayed image. At this time no theoretical model for this interaction has yet been put forth.

To further demonstrate the subsistence of a coherent vortex substructure along the stagnation zone, motion pictures were shot when smoke was injected in exactly the same way at two stations 15·24 cm apart. A representative sequence of 4 frames extending over a time interval $t = 116\frac{2}{3}$ ms along with their corresponding digitized sketches is given in figure 6 (plate 11). In this figure T/D designates the top view of the double-smoke injection and the scale of the schematics is 1:4. Similar cross-vortex tubes with nearly identical envelopes are perceived in all the images. These envelopes, based on the prescribed scale, ranged from about 20 to 40 mm. The existence of a coherent array consisting of regularly distributed cross-vortex tubes of about the same scales along the span of the stagnation zone is thus substantiated by the visualized flow pattern.

5.3. *Rear views*

Several motion pictures were shot looking upstream into the oncoming flow from a position downstream and slightly above the cylinder for obtaining a picture of the flow pattern in the x_1, x_3 plane (the cross plane). The goal was to observe the tilting of a stretched cross-vortex tube around the cylinder, the interaction of the amplified vorticity (or turbulence) with the laminar boundary layer and, finally, the ensuing turbulent boundary layer. A representative sequence of 16 stills from a ciné film extending over a time span of $666\frac{2}{3}$ ms and their digitized schematic diagrams are shown in figures 7 (a)–(d) (plates 12–15). In these figures R stands for rear view and the scale of the sketches is 3:10. The time span was estimated by tracking the evolution of a cross-vortex tube from the beginning of its winding over the cylinder until the full manifestation of a distinct spiral pattern suggestive of the growth of a turbulent boundary layer.

The flow pattern observed in the cross plane is that of an oncoming cross-vortex tube that undergoes gradually increasing tilting. At $t = 41\frac{2}{3}$ ms (frame 1-R, figure 7a) the axis of the cross-vortex tube is apparently in the x_1 direction. On the other hand, the pattern of the pathlines exhibited in sketch 2-R ($t = 83\frac{1}{3}$ ms, figure 7a) points out the inception of the tilting as the axis of the cross-vortex tube turns in the x_2 direction. With increasing time, the continuous veering of the cross-vortex tube axis away from its original cross direction (x_1 direction) toward the downstream direction (x_2 direction) is revealed by the gradual realization of a sharp vortex pattern in the cross plane. The pointing of the vortex-tube axis in the streamwise direction, indicative of the attainment of the final tilting of a stretched cross-vortex tube, is perceived starting from $t = 208\frac{1}{3}$ ms (frame 5-R, figure 7b).

The lateral spatial scales of the tilted cross-vortex tube, estimated according to the specified scale, ranged from about 7 to 42 mm as outlined in figures 7(a)–(d). They are generally of the same magnitude as their counterparts in both the stream and normal planes (x_1, x_2 and x_2, x_3 planes). Further inspection of the time evolution of the flow events in the cross plane reveals an expansion of the scales of the tilted cross-vortex tube followed by its interaction with the laminar boundary layer and the subsequent development of a turbulent boundary layer. The expansion indicates the outward diffusion of the amplified vorticity concentrated within a tilting cross-vortex tube. This outward diffusion of vorticity leads to a gradual disintegration of the coherent structure of the vortex tubes. The diffusing vorticity (or turbulence) fosters the development of a turbulent boundary layer which, in turn, promotes the break-up of the incoming coherent vortex tubes.

The flow evolution disclosed by the rear views lends support to the proposed mechanism for the generation of a turbulent boundary layer. A continuous widening of the large lateral scale from about 24 to 42 mm is discerned within the time interval $t = 83\frac{1}{3}$ to $333\frac{1}{3}$ ms (frames 2-R to 8-R, figures 7a, b). Invasion of the large-scale vorticity into the laminar boundary layer is first detected at about $t = 333\frac{1}{3}$ to 375 ms (frames 8-R and 9-R, figures 7b, c). This penetration of the tracked cross-vortex tube into the laminar boundary layer unveiled by a growing spiral pattern persists throughout the entire time cycle (until $t = 666\frac{2}{3}$ ms, frame 16-R, figure 7d). Most pre-eminent are the lateral spreading and the streamwise distension of the spiralling with increasing time exhibited by the pathlines depicted in sketches 10-R to 16-R ($t = 416\frac{2}{3}$ to $666\frac{2}{3}$ ms, figures 7c, d). Thus, the observed flow pattern in the cross plane reveals that the oncoming amplified vorticity interacts with the prevailing laminar boundary layer and induces its conversion into a turbulent boundary layer.

6. Concluding remarks

A visualization study of the flow around a circular cylinder was conducted for the sake of obtaining an overall physical confirmation of the explanation advanced by the vorticity-amplification theory with regard to the amplification of turbulence in stagnation flow and its effects upon the body boundary layer. The visualization was performed using titanium dioxide white smoke at a single cylinder-diameter Reynolds number of 8×10^3 owing to time constraints. Turbulence was superimposed in a controlled manner at scales larger than the neutral wavelength of the vorticity-amplification theory by means of an adequate turbulence-generating grid. A frame-by-frame scrutiny of the film strips led, despite its limitations, to the acquisition of a reasonably

quantitative interpretation of the gross flow structure in addition to supplying an in-depth qualitative perception of the flow patterns.

The visualization provided evidence verifying: (1) the selective stretching of cross-vortex tubes which is responsible for the amplification of cross vorticity and, hence, of streamwise turbulence ahead of the body boundary layer; (2) the streamwise biased tilting of cross-vortex tubes; (3) the existence of a coherent vortex flow sub-structure near the stagnation zone; (4) the interaction of the amplified vorticity with the laminar boundary layer; and, finally, (5) the development of a turbulent boundary layer. These results indicate that adequate control of the stretching and tilting of oncoming vorticity can lead to management of the nature of the body boundary layer.

The work reported here is part of a research programme on the structure of turbulence and the effects of the turbulence in flow about bluff bodies and aerodynamic surfaces being conducted at the Fluid Dynamics and Diffusion Laboratory, Colorado State University. Sponsoring of this research programme by N.A.S.A. Lewis Research Center and Project SQUID (Office of Naval Research) is gratefully acknowledged.

REFERENCES

BEARMAN, P. W. 1972 Some measurements of the distortion of turbulence approaching a two-dimensional bluff body. *J. Fluid Mech.* **53**, 451–467.

DEAN, R. C. 1955 Aerodynamic measurements. *Gas Turbine Lab. Rep.* pp. 61–65. Massachusetts Institute of Technology.

HUNT, J. C. R. 1973 A theory of turbulent flow round two-dimensional bluff bodies. *J. Fluid Mech.* **61**, 625–706.

HURD, C. W., CHESKY, K. P. & SHAPIRO, A. H. 1953 Influence of viscous effects on impact tubes. *Trans. A.S.M.E., J. Appl. Mech.* **20**, 253–256.

KESTIN, J. 1966 The effect of freestream turbulence in heat transfer rates. *Advances in Heat Transfer*, vol. 3, pp. 1–32. Academic.

KESTIN, J., BRUN, E. & DIEP, G. B. 1966 Sur un nouveau type de tourbillons longitudinaux dans l'écoulement autour d'un cylindre. *C. R. Acad. Sci. Paris* A **263**, 742–745.

KESTIN, J. & MAEDER, P. F. 1957 Influence of turbulence on the transfer of heat from cylinders. *N.A.C.A. Tech. Note* 4018.

KESTIN, J. & WOOD, R. T. 1970 On the stability of two-dimensional stagnation flow. *J. Fluid Mech.* **44**, 461–479.

OWER, E. & PANKHURST, R. C. 1966 *The measurement of airflow*, 4th edn, p. 46. Pergamon.

PIERCY, N. A. & RICHARDSON, E. G. 1928 The variation of velocity amplitude close to the surface of a cylinder moving through a viscous fluid. *Phil. Mag.* **6**, 970–977.

PIERCY, N. A. V. & RICHARDSON, E. G. 1930 The turbulence in front of a body moving through a viscous fluid. *Phil. Mag.* **9**, 1038–1040.

ROSHKO, A. 1954 On the development of turbulent wakes from vortex streets. *N.A.C.A. Tech. Rep.* 1191.

SADEH, W. Z., SUTERA, S. P. & MAEDER, P. F. 1970*a* Analysis of vorticity amplification in the flow approaching a two-dimensional stagnation point. *Z. angew. Math. Phys.* **21**, 669–716.

SADEH, W. Z., SUTERA, S. P. & MAEDER, P. F. 1970*b* An investigation of vorticity amplification in stagnation flow. *Z. angew. Math. Phys.* **21**, 717–742.

SCHLICHTING, H. 1968 *Boundary-layer theory*, 6th edn, pp. 154–162. McGraw-Hill.

SUTERA, S. P. 1965 Vorticity amplification in stagnation-point flow and its effect on heat transfer. *J. Fluid Mech.* **21**, 513–534.

SUTERA, S. P., MAEDER, P. F. & KESTIN, J. 1963 On the sensitivity of heat transfer in the stagnation-point boundary layer to free-stream vorticity. *J. Fluid Mech.* **16**, 497–520.

TAYLOR, G. I. 1938 The spectrum of turbulence. *Proc. Roy. Soc.* A **164**, 476–490.

TRACI, R. M. & WILCOX, D. C. 1975 Freestream turbulence effects on stagnation point heat transfer. *A.I.A.A. J.* **13**, 890–896.

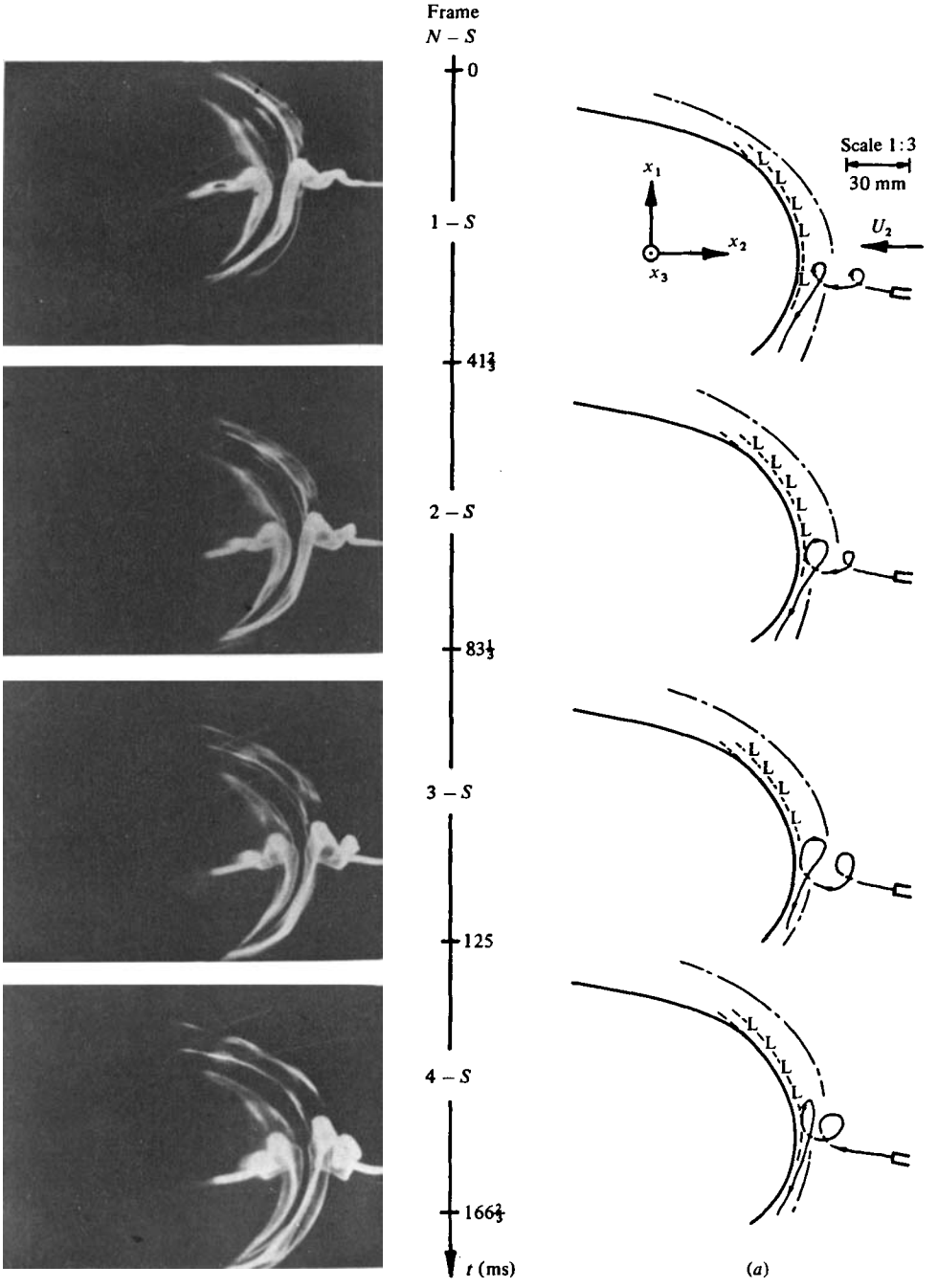

FIGURE 4. Side-view sequence illustrating the time history of a tracked cross-vortex tube viewed in the x_1, x_2 plane (the stream plane).

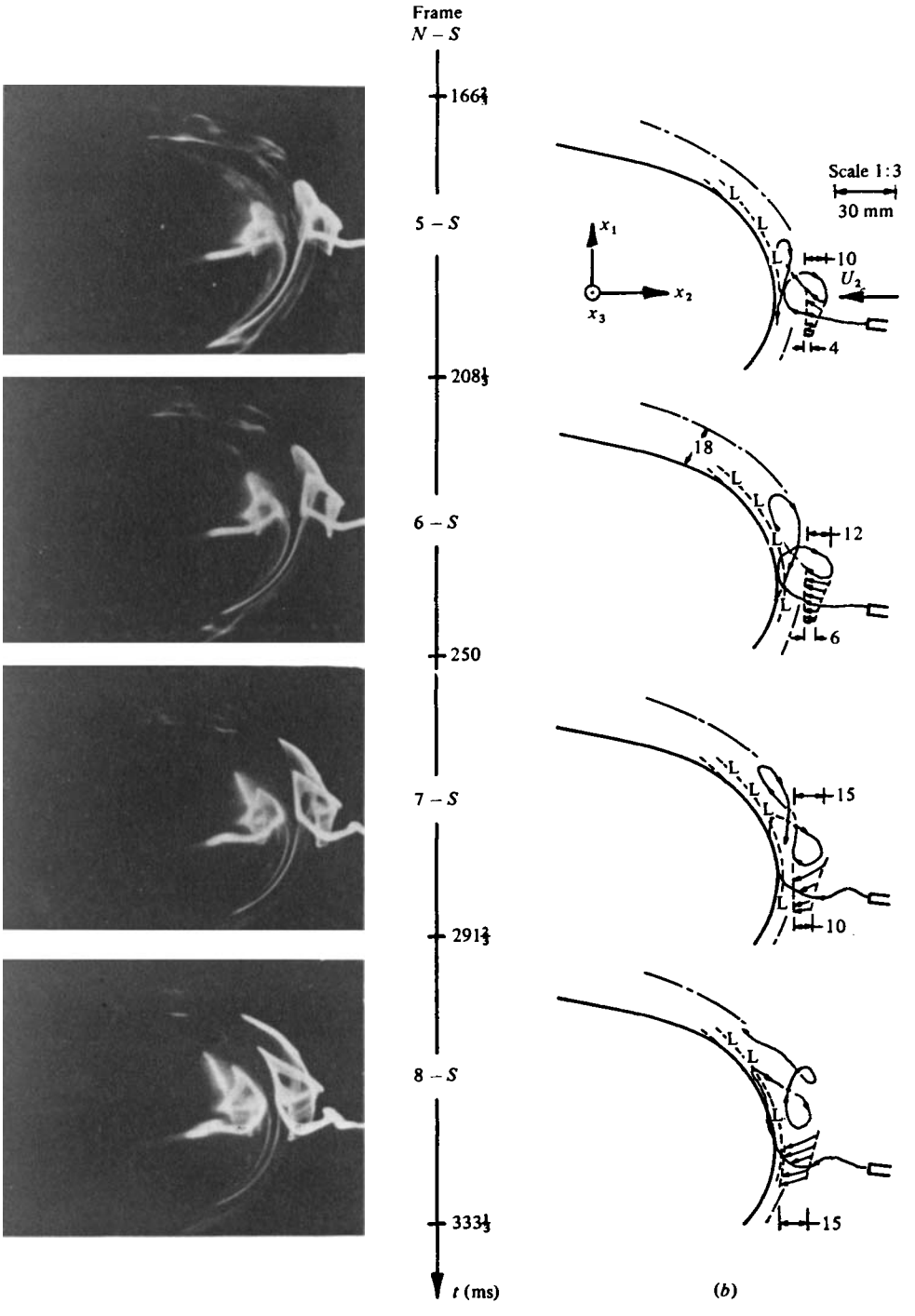
Frame
N – S
166⅔
5 – S
208⅓
6 – S
250
7 – S
291⅔
8 – S
333⅓
t (ms)
Scale 1:3
30 mm
x_1
x_2
x_3
U_2
L
10
4
18
12
6
15
10
15
(b)

FIGURE 4(*b*)

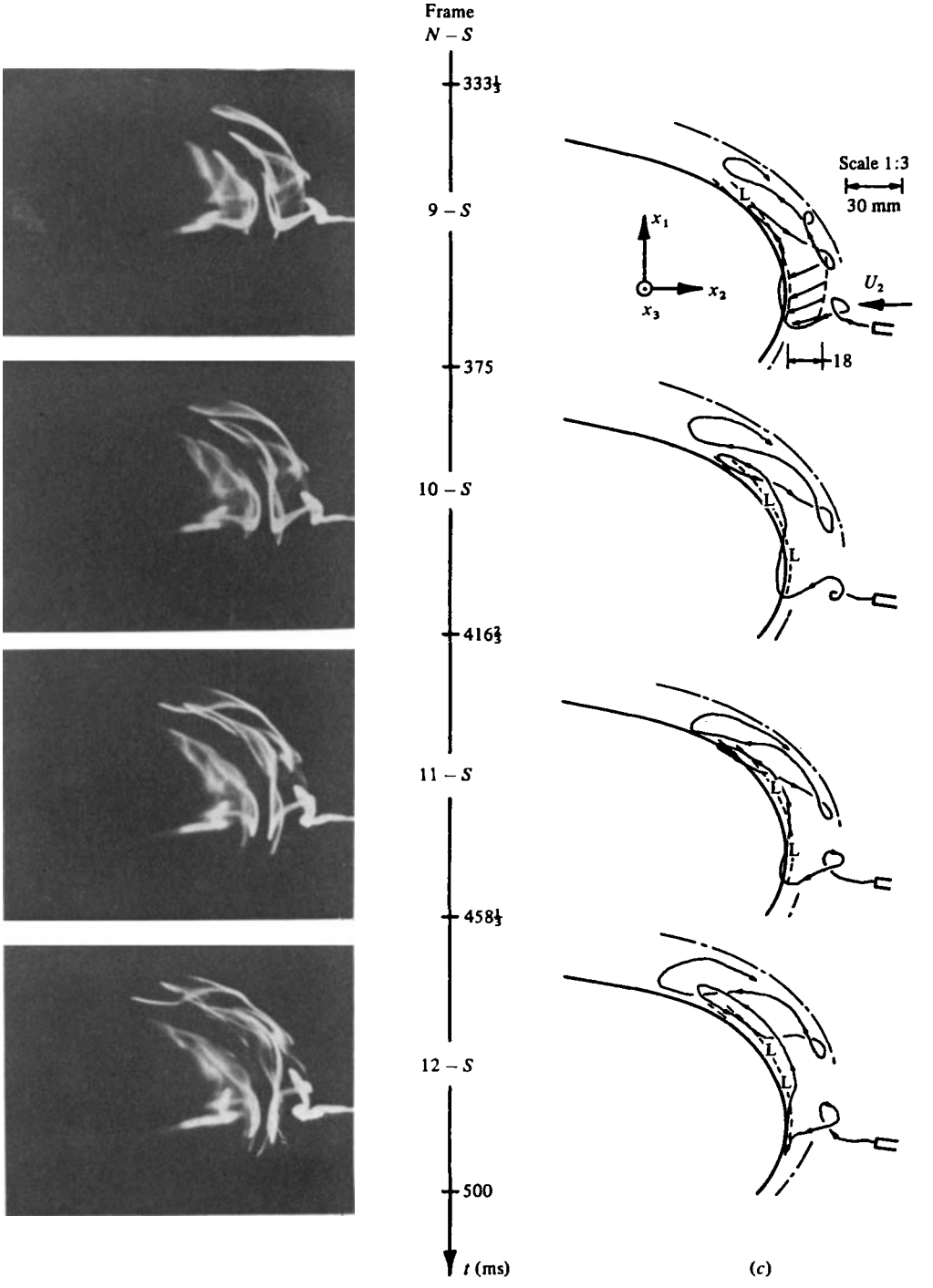
Frame
N – S
333⅓
9 – S
375
10 – S
416⅔
11 – S
458⅓
12 – S
500
t (ms)
Scale 1:3
30 mm
x_1
x_2
x_3
U_2
18
L
(c)

FIGURE 4 (*c*)

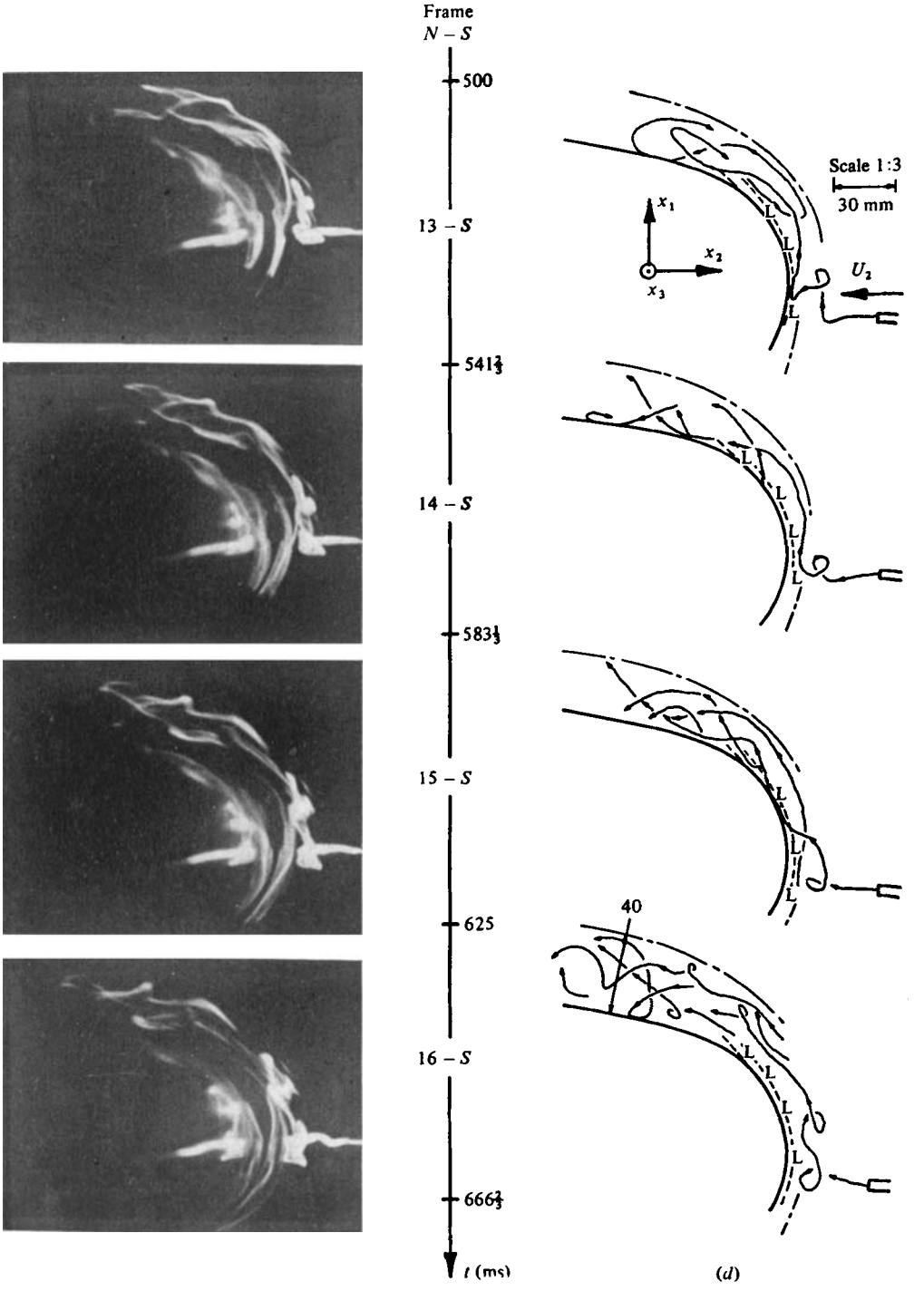
Frame
N – S
500
13 – S
541⅔
14 – S
583⅓
15 – S
625
16 – S
666⅔
t (ms)
Scale 1:3
30 mm
x_1
x_2
x_3
U_2
L
40
(d)

FIGURE 4(*d*)

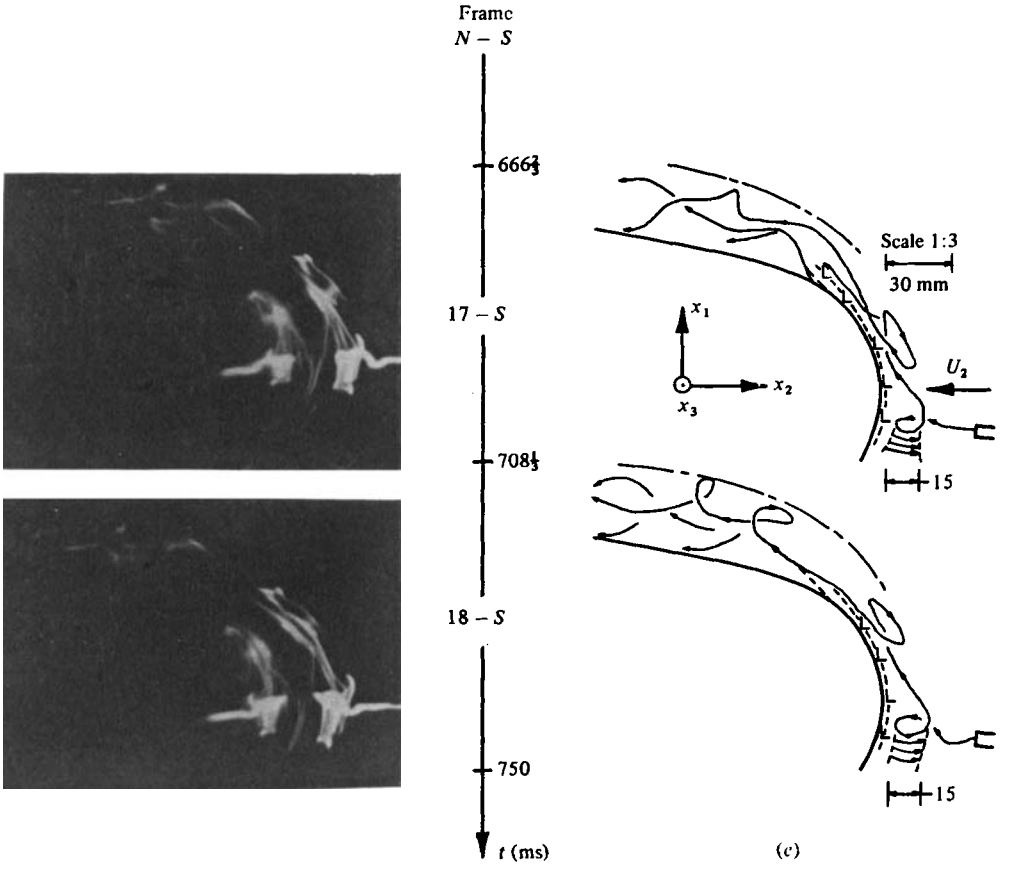
Frame
N – S
666⅔
17 – S
708⅓
18 – S
750
t (ms)
Scale 1:3
30 mm
x_1
x_2
x_3
U_2
15
15
(c)

FIGURE 4 (*e*)

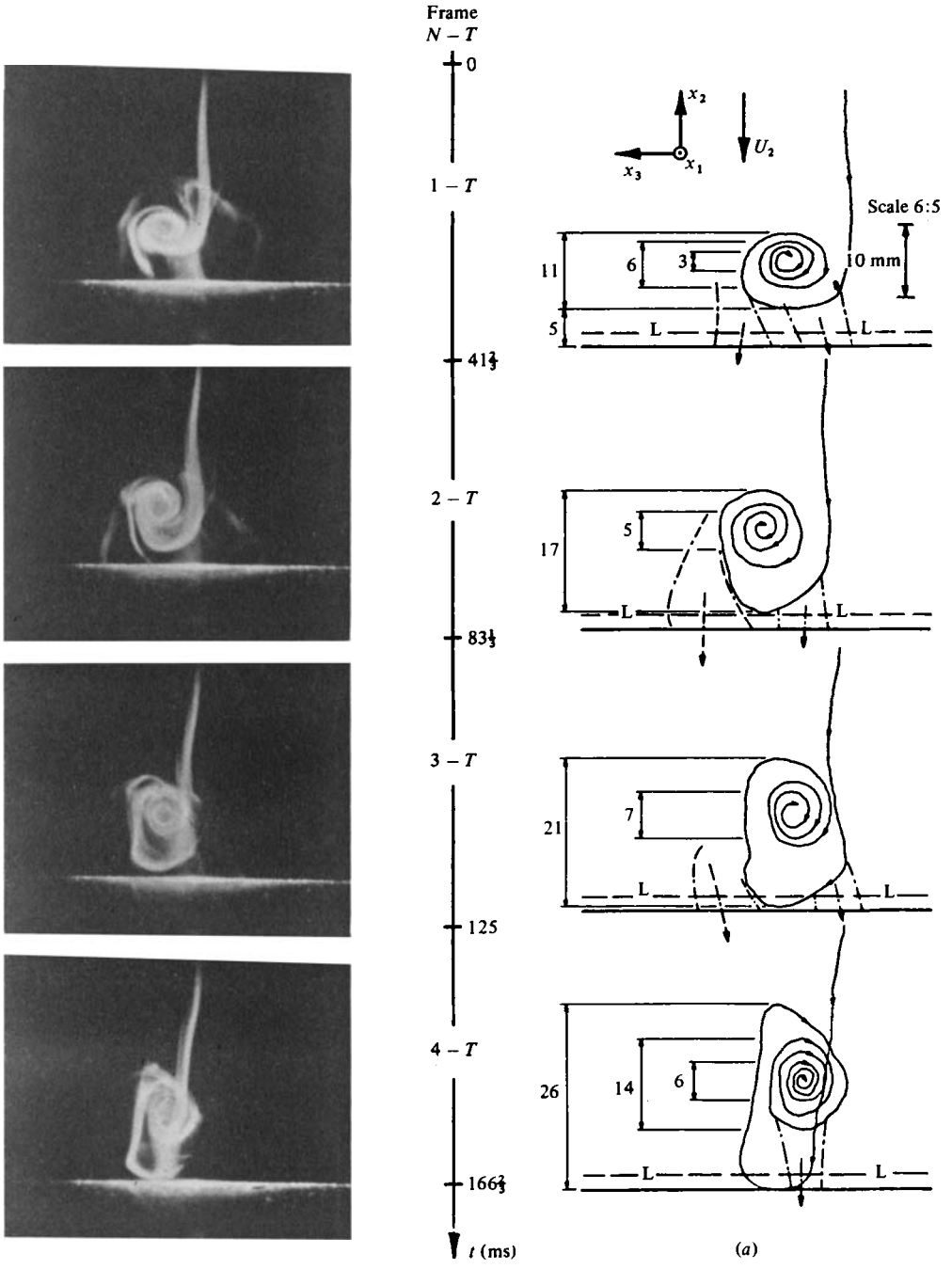

FIGURE 5. Top-view sequence illustrating the evolution of a standing cross-vortex tube near the stagnation zone viewed in the x_2, x_3 plane (the normal plane).

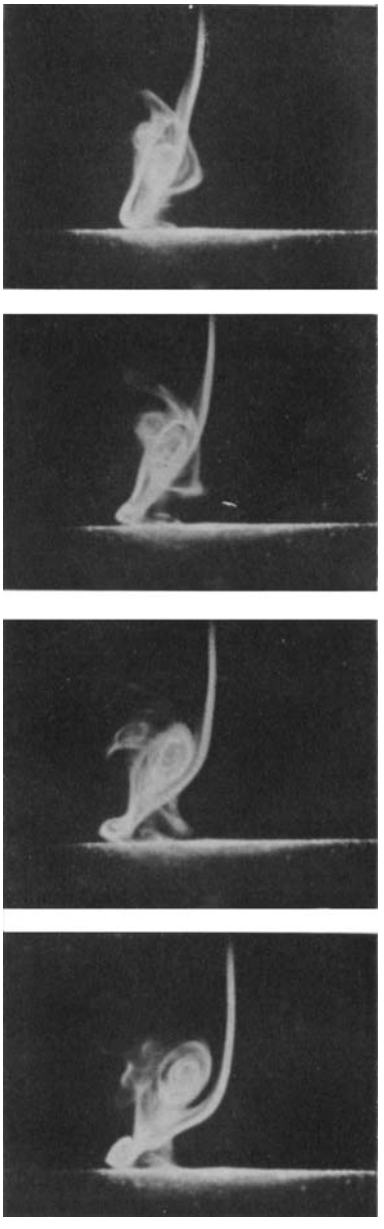

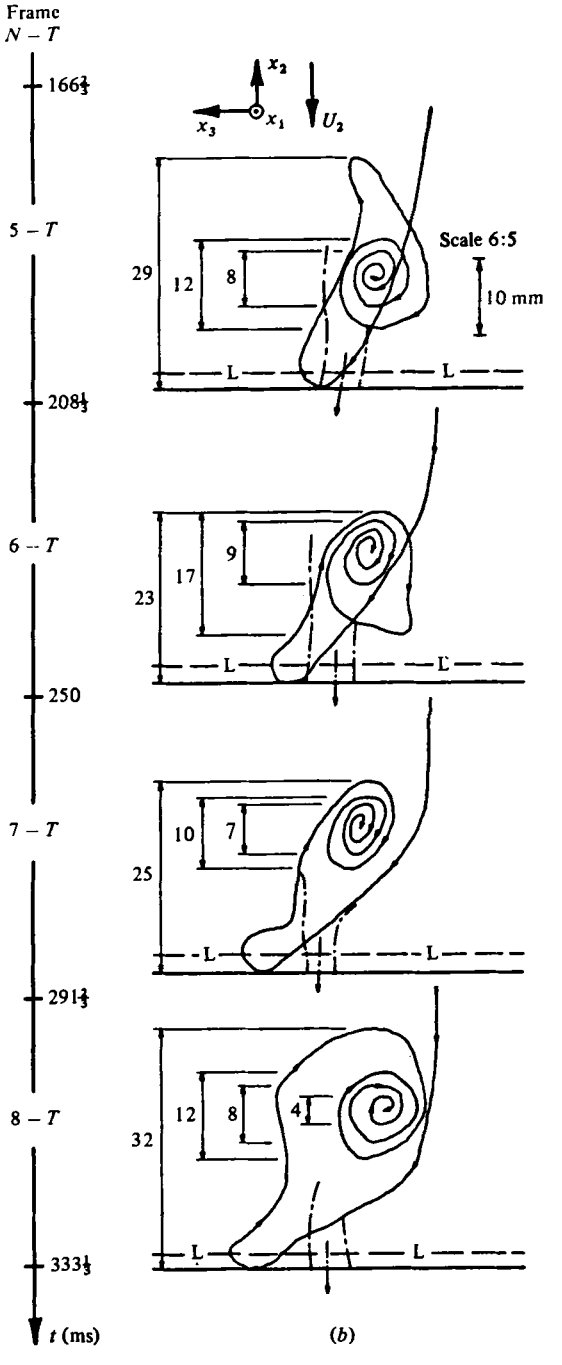
Frame
N – T
166⅔
5 – T
208⅓
6 – T
250
7 – T
291⅔
8 – T
333⅓
t (ms)
x2
x1
x3
U2
Scale 6:5
10 mm
29
12
8
L
L
23
17
9
L
L
25
10
7
L
L
32
12
8
4
L
L
(b)

FIGURE 5(*b*)

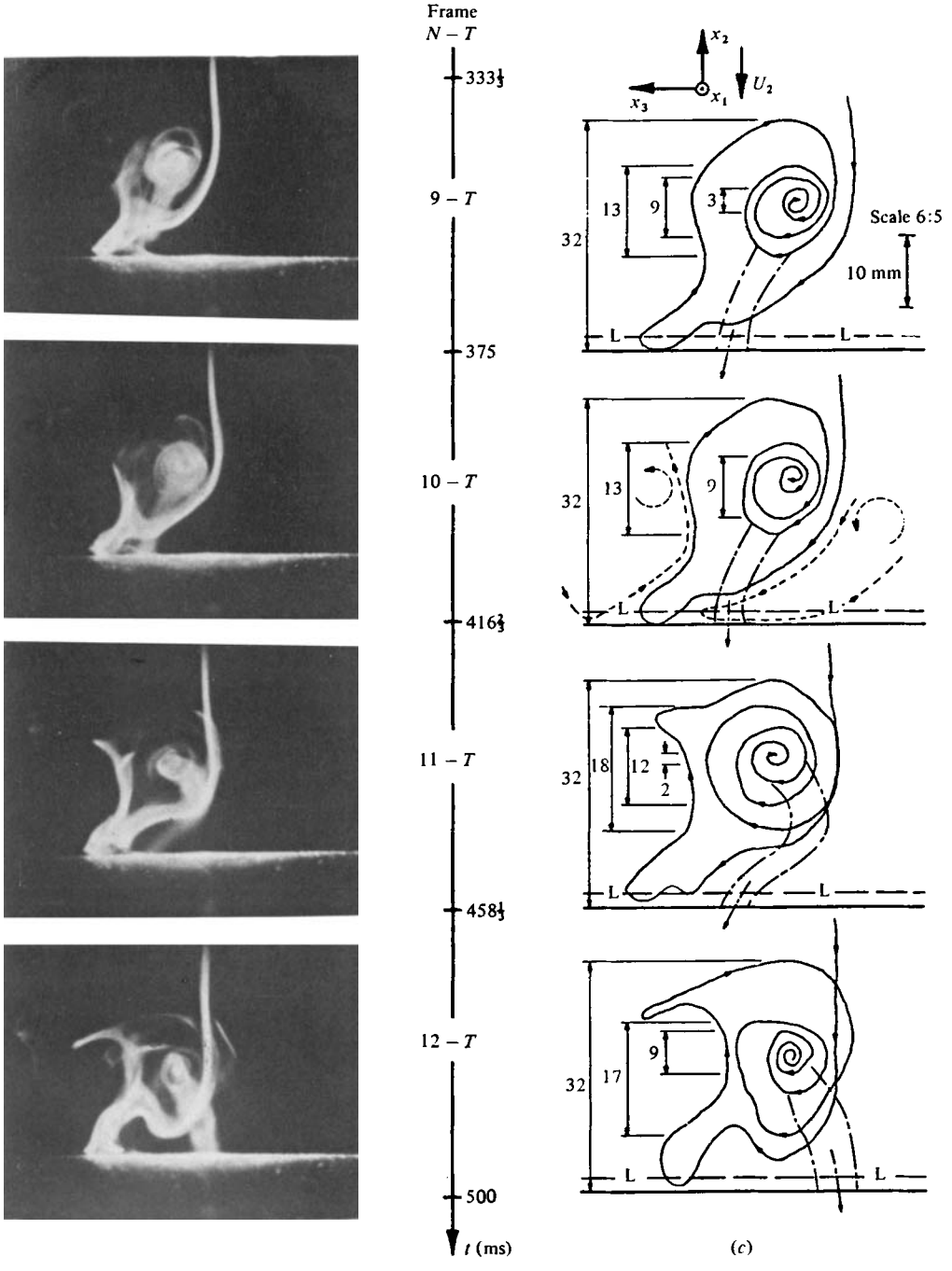
Frame
N – T
333⅓
9 – T
375
10 – T
416⅔
11 – T
458⅓
12 – T
500
t (ms)
x2
x1
x3
U2
Scale 6:5
10 mm
32
13
9
3
L
18
12
2
17
(c)

FIGURE 5(c)

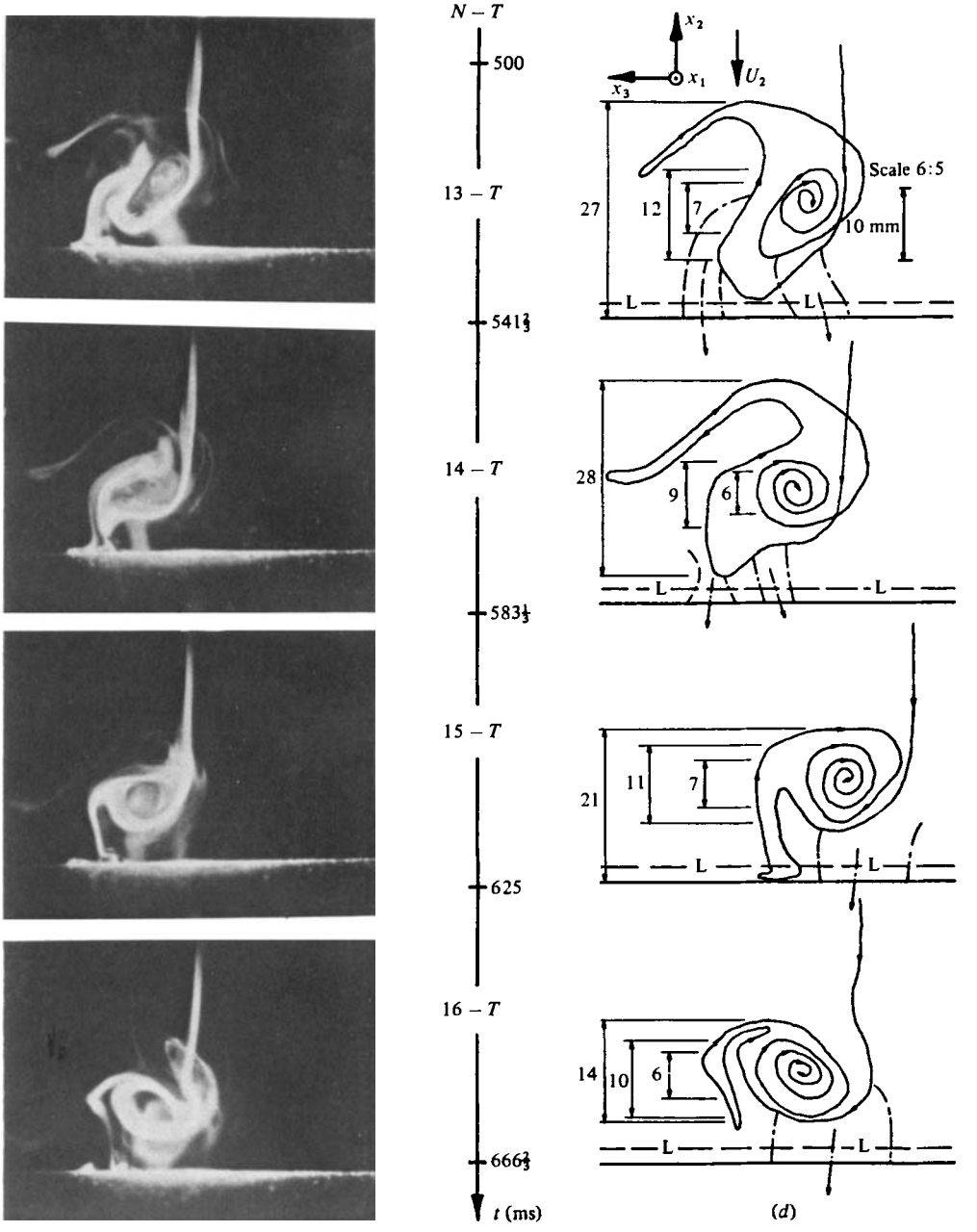
Frame
N – T
500
13 – T
541⅔
14 – T
583⅓
15 – T
625
16 – T
666⅔
t (ms)
x2
x1
x3
U2
Scale 6:5
10 mm
27
12
7
28
9
6
21
11
7
14
10
6
L
(d)

FIGURE 5(*d*)

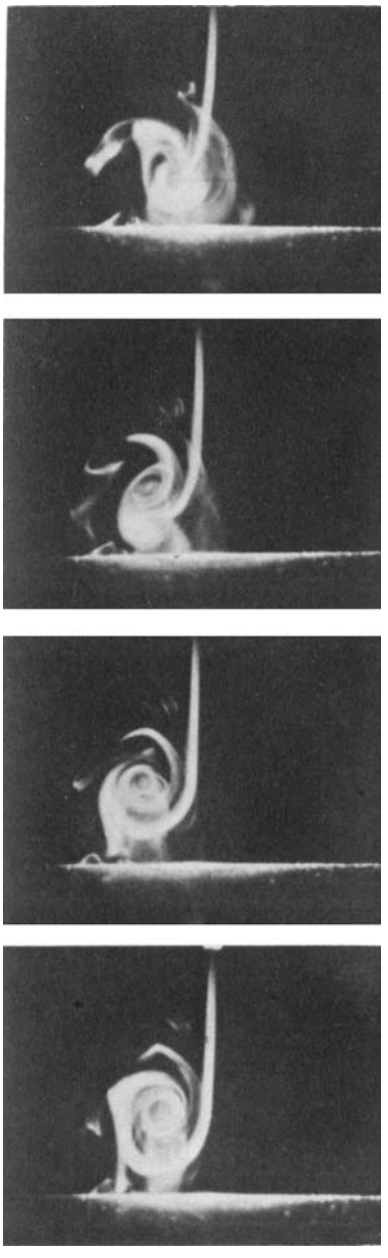
Frame
N – T
666⅔
17 – T
708⅓
18 – T
750
19 – T
791⅔
20 – T
833⅓
t (ms)
x2
x1
x3
U2
Scale 6:5
10 mm
20
12
7
L
L
9
7
L
L
18
11
L
L
12
7
3
5
L
L

(e)

FIGURE 5(e)

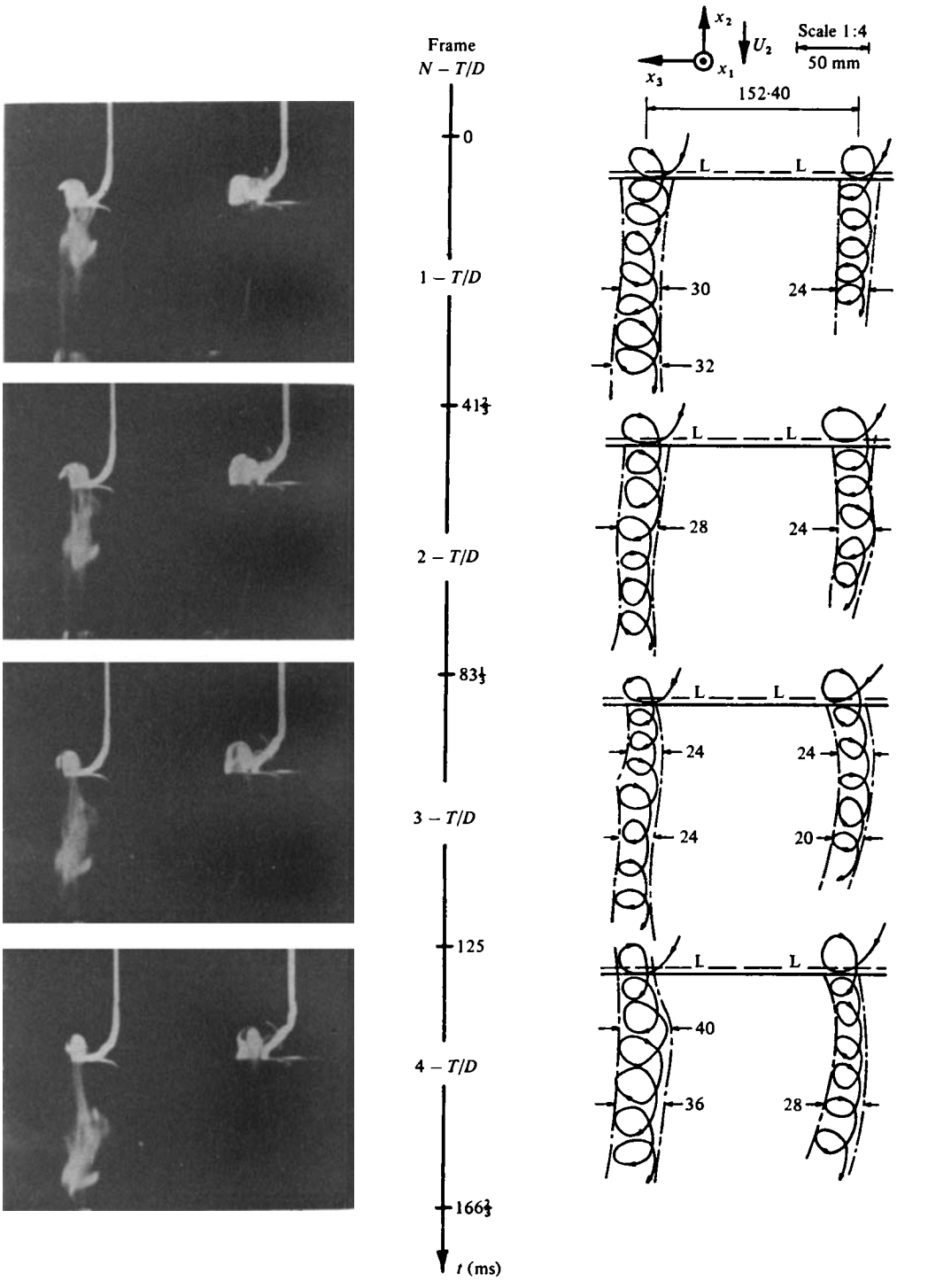

FIGURE 6. Top-view sequence illustrating the coherent vortex flow pattern along the stagnation-zone span and the winding of the stretched cross-vortex tubes over the cylinder viewed in the x_2, x_3 plane (the normal plane).

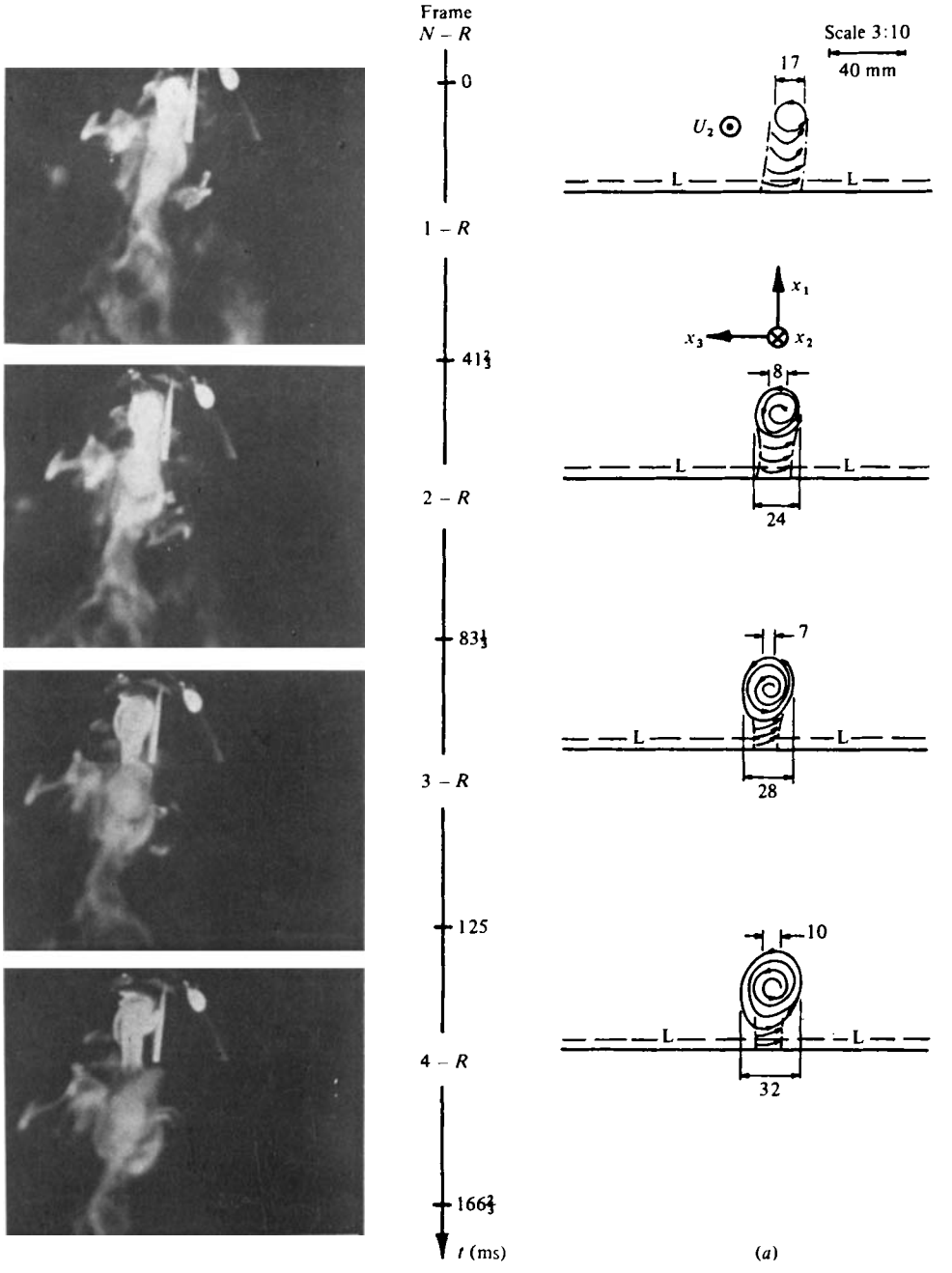

FIGURE 7. Rear-view sequence illustrating the tilting of a stretched cross-vortex tube and the growth of a turbulent boundary layer viewed in the x_1, x_3 plane (the cross plane).

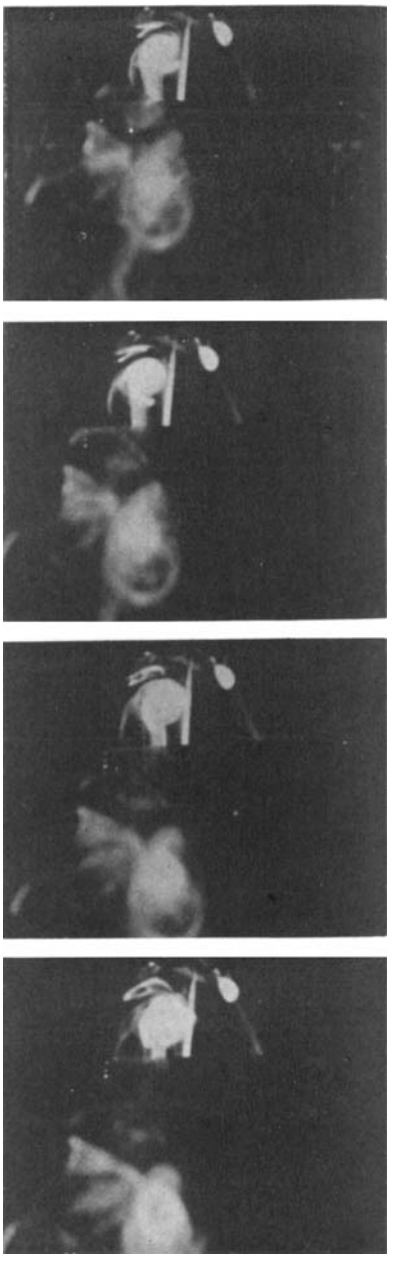

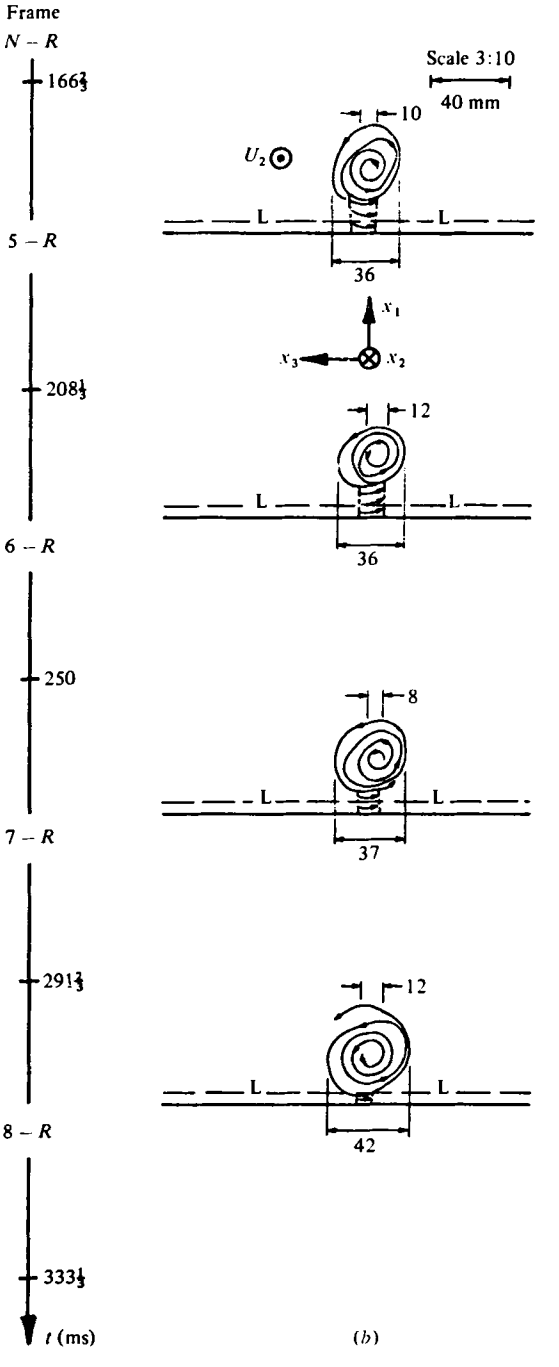
Frame
N – R
166⅔
5 – R
208⅓
6 – R
250
7 – R
291⅔
8 – R
333⅓
t (ms)
Scale 3:10
40 mm
10
U_2
L
L
36
x_1
x_3
x_2
12
L
L
36
8
L
L
37
12
L
L
42
(b)

FIGURE 7 (*b*)

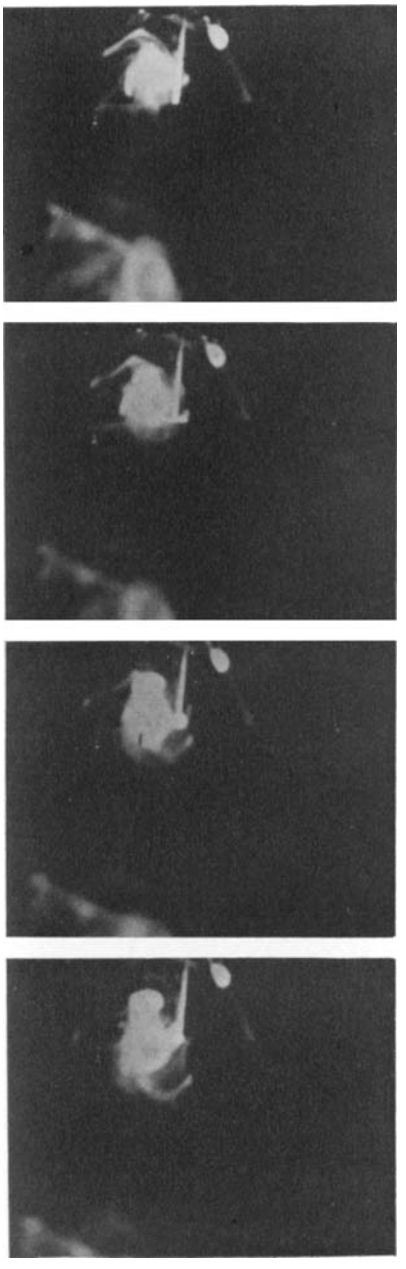

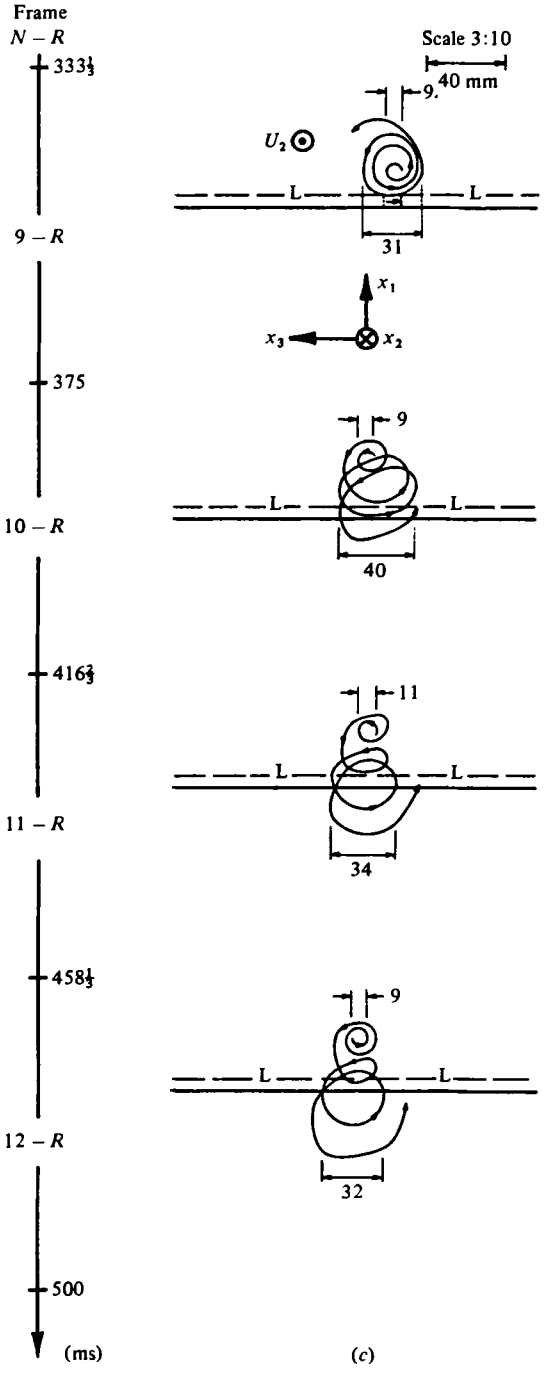
Frame
N – R
333⅓
9 – R
375
10 – R
416⅔
11 – R
458⅓
12 – R
500
(ms)
Scale 3:10
40 mm
9
U_2
L
L
31
x_1
x_3
x_2
9
L
L
40
11
L
L
34
9
L
L
32
(c)

FIGURE 7 (*c*)

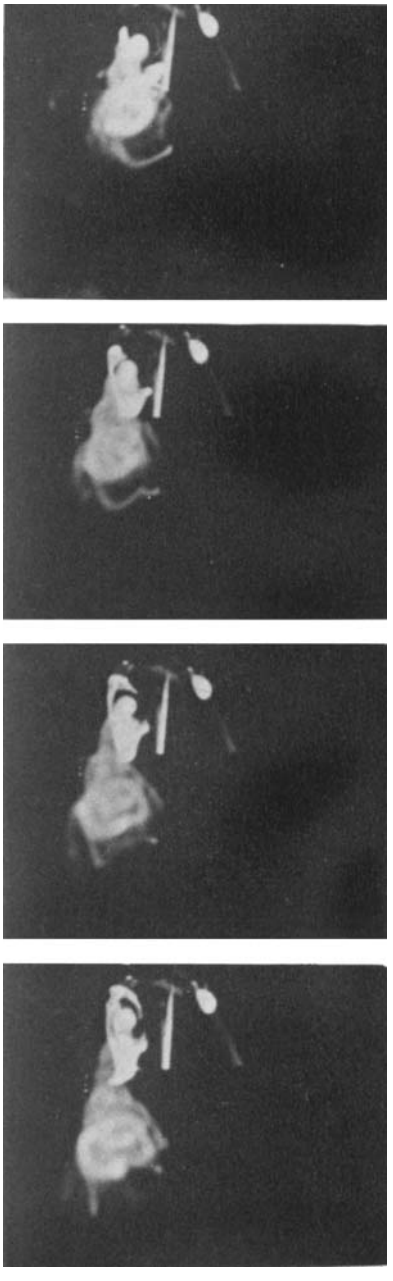

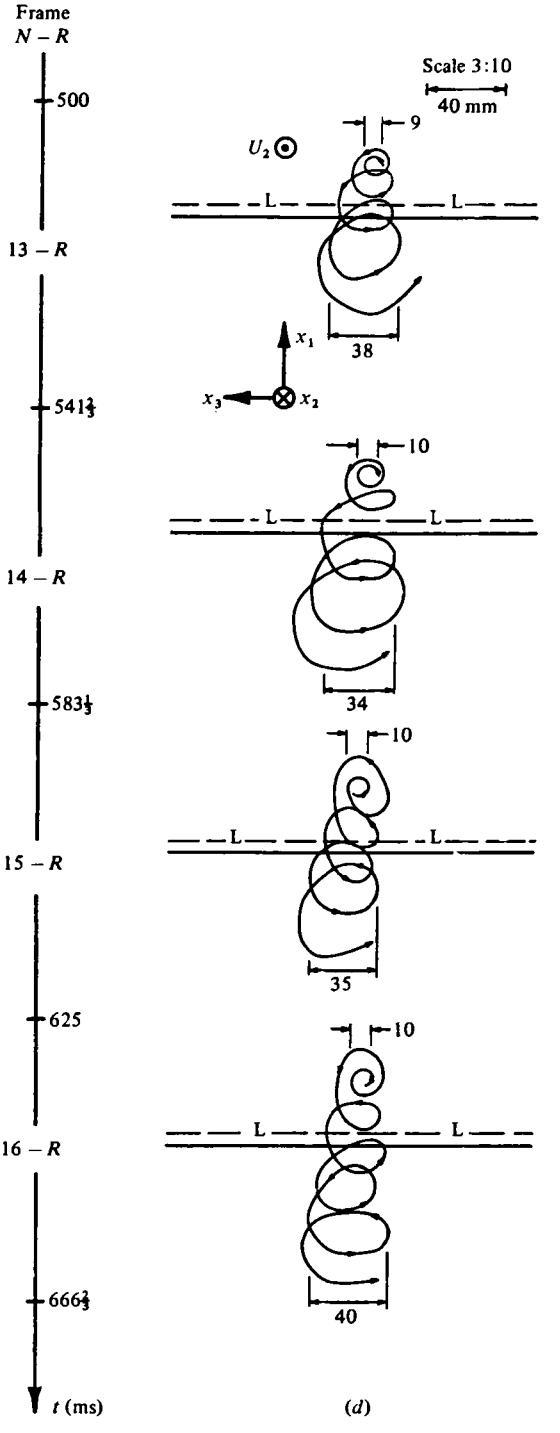
Frame
N – R
500
13 – R
541⅔
14 – R
583⅓
15 – R
625
16 – R
666⅔
t (ms)
Scale 3:10
40 mm
9
U_2
L
L
x_1
38
x_3
x_2
10
L
L
34
10
L
L
35
10
L
L
40
(d)

FIGURE 7(*d*)